HHS Public Access

Author manuscript

Small. Author manuscript; available in PMC 2021 May 01.

Published in final edited form as:

Small. 2020 May ; 16(20): e1907150. doi:10.1002/smll.201907150.

Active Delivery of VLPs Promotes Anti-Tumor Activity in a Mouse Ovarian Tumor Model

Chao Wang[1], **Berta Esteban Fernández de Ávila**[1], **Rodolfo Mundaca-Uribe**[1], **Miguel Angel Lopez-Ramirez**[1], **Doris E. Ramírez-Herrera**[1], **Sourabh Shukla**[1], **Nicole F. Steinmetz**[1,2,3,4,5,*], **Joseph Wang**[1,5,*]

[1]Department of NanoEngineering, University of California San Diego, La Jolla, CA 92093, USA.

[2]Bioengineering, University of California San Diego, La Jolla, CA 92093, USA.

[3]Radiology, University of California San Diego, La Jolla, CA 92093, USA.

[4]Moores Cancer Center, University of California San Diego, La Jolla, CA 92093, USA.

[5]Center for Nano-Immunoengineering, University of California San Diego, La Jolla, CA 92093, USA.

Abstract

Virus-like nanoparticles (VLPs) have been used as an attractive means in cancer immunotherapy because of their unique intrinsic immunostimulatory properties. However, for treating metastatic tumors in the peritoneal cavity, such as ovarian cancer, multiple injections of therapy are needed due to the large peritoneal space and fast excretion of therapy. Here, we report on the development of active VLP delivery vehicles for the treatment of peritoneal ovarian tumors using biocompatible Qβ VLPs-loaded Mg-based micromotors. The autonomous propulsion of such Qβ VLPs-loaded Mg-micromotors in the peritoneal fluid enables active delivery of intact immunostimulatory Qβ VLPs to the peritoneal space of ovarian tumor bearing mice, greatly enhancing the local distribution and retention of Qβ VLPs. Such improved distribution and longer retention time of Qβ in the peritoneal cavity leads to enhanced immunostimulation and therefore increased survival rate of tumor-bearing mice compared to a passive Qβ treatment. For clinical translation, the active delivery of VLPs holds great promise for tumor immunotherapy towards the treatment of different types of primary and metastatic tumors in the peritoneal cavity.

Keywords

virus-like particles; immunotherapy; micromotor; active delivery; ovarian tumor

*Correspondence to: nsteinmetz@ucsd.edu and josephwang@ucsd.edu.

Author Contributions

The manuscript was written through contributions of all authors. All authors have given approval to the final version of the manuscript.

The authors declare no competing financial/commercial interests.

Supporting Information

Supporting Information is available from the Wiley Online Library or from the author.

1. Introduction

Immunotherapy is emerging as an attractive strategy and has demonstrated clinical benefits in a variety of cancers. The promise of immunotherapy relies in its ability to re-model the suppressive tumor microenvironment and to promote anti-tumor immunity.[1,2] Virus-like nanoparticles (VLPs) have been considered as an attractive tool for stimulating immune responses, either when used as vaccines or immunotherapies. For example, VLPs derived from hepatitis B virus and human papillomavirus are able to promote immunogenicity and have been developed and approved as human vaccines to protect patients from infectious-disease associated tumors.[3,4] VLPs from Cowpea mosaic virus (CPMV), when administered *in situ* directly into an identified tumor, show potent systemic anti-tumor immunity in several tumor mouse models[5–7] and canine patients.[8] VLPs from bacteriophages, such as Qβ and MS2, also show immunostimulatory properties and have been developed as a platform for delivery of vaccine to human and animals.[9–11]

In this work, we developed a micromotor-based active delivery strategy for a VLP immunotherapy targeting ovarian cancer. Ovarian cancer is an ideal target for immunotherapies, because these tumors are generally immunogenic providing tumor-associated antigens.[12] Therefore, instead of employing custom-made antigen or neoantigen as a traditional vaccination strategy, an ideal efficacy can be achieved by directly using the tumor itself as a source of antigen. However, the large peritoneal space where metastatic tumors usually appear requires high doses and repeated administration of drugs or therapy to activate immune system before being washed out.[13]

Over the past years, synthetic active nano/microvehicle delivery systems − defined as nano/micromotors − have been explored for the loading, transport and active delivery of a variety of different cargoes towards different biomedical applications.[14–19] Different designs of nano/micromotors based on biocompatible materials, such as zinc (Zn) or magnesium (Mg), have been reported, showing considerable potential for enhanced transport, delivery and retention of therapeutic cargoes in different body locations.[20–23] The spontaneous reaction of the Zn or Mg micromotor with acid- or water-based biofluids of different pH results in a rapid release of hydrogen bubbles from an exposed side of the micromotor, inducing the fast micromotor movement.[20] These biocompatible and biodegradable nano/micromotors offer significant advantages for *in vivo* operation, including self-propulsion in biological fluids, active cargo distribution, specific activation in the target environment and high loading capacity, and self-destruction. Overall, the active delivery provided by such nano/micromotors results in greatly improved cargo delivery and enhanced tissue penetration in the target area. We hypothesized that the design of biodegradable micromotors for the active delivery of VLPs would provide faster VLPs release in the peritoneal area with improved tumor retention and thus enhanced anti-tumor response.

Herein, we report the fabrication, characterization, advantages and *in vivo* application of a biocompatible and biodegradable Qβ VLP-loaded Mg-based micromotor (denoted as Qβ-motor) as an active and dynamic Qβ VLP delivery platform towards the eradication of ovarian cancer. Ascites is a key clinical symptom in ovarian cancer patients. The weak acidic peritoneal fluid provides an applicable space for motor-based therapy given the spontaneous

reaction of Mg with this medium which generates hydrogen bubbles that results in efficient motor propulsion in acidic environments. We took advantage of such efficient autonomous motion of biocompatible Mg-based micromotors in biological fluids to actively deliver Qβ VLP payloads within the tumor area. Such motor propulsion enables active delivery of the Qβ VLP payload in the tumor microenvironment that greatly enhances the local distribution and retention time of such Qβ VLPs in the tumor towards improved immunotherapy.

2. Results

Figure 1a illustrates a schematic displaying the overall concept of employing Mg-based micromotors for the active release of Qβ VLPs in an ovarian tumor mouse model. The fabrication steps of the Qβ-motors are schematically illustrated in Figure 1b by a layer-by-layer fashion. The core of the micromotors is comprised of a biocompatible and biodegradable Mg microparticle 'engine' with an average size of ~25 μm, which are initially dispersed onto a glass slide (Figure 1b, I). Subsequently, a fast and short gold sputter deposition over the Mg microparticles, attached to the surface of the glass slide, takes place (Figure 1b, II). The Au layer is important to allow an efficient micromotor chemical reaction with the water fuel to generate hydrogen bubbles in biological media. Such reaction and corresponding bubble generation are attributed to the combination of enhanced macrogalvanic corrosion (Au layer) and the presence of chloride ions essential for pitting corrosion.[24] Moreover, the deposition of an asymmetric coating with a thin layer of TiO_2 was performed by using atomic layer deposition (ALD) (Figure 1b, III). Such ALD process leads to a uniform TiO_2 shell over the Mg microparticles, while leaving a small opening of ~2 μm at the Mg sphere-glass contact point, essential in the formation of the Janus motor structure and further interaction between the exposed Mg core and the intraperitoneal (IP) fluid. Such interaction leads to a spontaneous reaction and generation of hydrogen bubbles on this exposed area, resulting in a directional continuous micromotor motion. The Mg/Au/TiO_2 Janus micromotors were then coated with two PLGA films to ensure the stability of the TiO_2 coating when forming the chitosan layer (Figure 1b, IV). Furthermore, the Mg/Au/TiO_2/PLGA micromotors were then coated with a thin chitosan film containing the Qβ VLP payload (Figure 1b, V). Finally, the resulting Qβ VLP-loaded micromotors were collected by soft scratching the glass slide and stored at 4°C until use (Figure 1b, VI) (see detailed experimental protocol in Experimental Section).

To verify the successful fabrication of the Qβ-motors, a scanning electron micrograph (SEM) was performed to fully characterize the morphology of the particles. SEM images of a Mg/Au/TiO_2/PLGA micromotor, Mg/Au/TiO_2/PLGA/Qβ-loaded Chitosan micromotor (Qβ-motor), the Au/TiO_2 shell of a Qβ-motor after being exposed to IP fluid, and corresponding Energy-dispersive X-ray spectroscopy (EDX) images are shown in Figure 1c (I-III, respectively), illustrating the distribution of elemental Mg (cyan), Au (yellow), Ti (magenta), N (green) and S (white). The SEM image of a Qβ-motor (Figure 1c, II) confirms the presence of the Qβ VLP-loaded chitosan coating over the Mg-based motor. In addition, the corresponding EDX analysis demonstrates the presence of N and S (in green and white, respectively) responsible of the presence of chitosan and Qβ VLPs. SEM and EDX images of the Au/TiO_2 shell of a Qβ-motor that was previously exposed to IP fluid clearly demonstrate the small opening (~2 μm) on one side of the spherical micromotor, produced

during the TiO_2 coating process (Figure 1c, III). The corresponding EDX images illustrate the absence of Mg, N and S due to the presence of the Qβ-motor within the IP fluid, inducing a spontaneous reaction with the Mg motor core and the dissolution of the chitosan coating with active Qβ VLP release. In acidic conditions (pH<6), the amino groups present in chitosan are partially protonated resulting in repulsion between positively charged macrochains and thus allowing diffusion of water molecules with chitosan film dissolution and posterior release of the therapeutic Qβ VLP payload.[25]

A fluorescence study was performed to further confirm the efficient Qβ VLP-loading within the chitosan coating. In this study, Cyanine3 dye (Cy3, λ_{em}=568 nm) labeled Qβ VLPs were synthesized using established protocols (see detailed experimental protocol in Experimental Section and Cy3-Qβ VLPs and Cy3-Qβ-motors characterization in the SI). In Figure S1, SDS gel and size exclusion chromatography (SEC) were used to confirm the successful conjugation of Cy3 on Qβ VLPs. Cy3-Qβ-motors were prepared following the same protocol described above but loading the chitosan film with Cy3-Qβ VLPs. Optical, fluorescence and merged images of Cy3-Qβ-motors are displayed in Figure 1d and Figure S2. The high red fluorescent intensity confirms the successful micromotor coating process of the micromotors with the Cy3-Qβ VLP loaded chitosan layer and reflects the high Qβ VLP-loading capacity the micromotors can withstand.

The ability of the Qβ-motors to efficiently propel in mouse IP fluid was tested *in vitro*. The Qβ-motors displayed fast, powerful and directional propulsion in the mouse IP fluid with an average speed of 60 μm/s (Figure 1e). The propulsion behavior of Qβ-motors was also compared to bare Mg/Au/TiO_2-motors and Mg/Au/TiO_2/PLGA/Chitosan-motors; as expected, bare Mg/Au/TiO_2-motors (without the PLGA and Qβ-loaded chitosan layers), displayed higher speed values (90 μm/s) in the same IP fluid, what was attributed to the absence of the protective PLGA and chitosan loading layers. However, no speed difference was observed between Mg/Au/TiO_2/PLGA/Chitosan-motors and Qβ-motors (Figure 1e, second *vs* third bar, respectively), suggesting that the Qβ VLP payload does not compromise the motor propulsion. The microscopic images in Figure 1f (taken from Video S1) illustrate the fast and prolonged autonomous propulsion of the different motor formulations (I-III: bare Mg/Au/TiO_2-motor, Mg/Au/TiO_2/PLGA/Chitosan-motor and Qβ-motor, respectively) in IP fluid. Such efficient propulsion is essential for the Qβ-motors to actively release the Qβ VLP payload from the chitosan loading layer in the tumor area in a faster fashion when compared to passive diffusion release.

Qβ is a 28 nm icosahedral bacteriophage that consists of 180 copies of identical capsid proteins.[26] Multiple characterization assays were conducted to compare the physicochemical properties of purified Qβ VLPs and Qβ VLPs released from micromotors. The concentrations of Qβ VLPs and Qβ VLPs released from motor were determined by bicinchoninic acid assay (BCA assay). 20 μg (7.94 pmol) of Qβ VLPs and Qβ VLPs released from motors (0.26 mg) were used for the following characterization. Native agarose gels showed nucleic acid bands colocalized with the protein bands, confirming the intact structure of the particles (Figure 2a and 2b; like other VLPs, Qβ VLPs are known to package host RNA). The coat protein composition was verified by SDS-PAGE analysis. SDS-PAGE showed a single band at ~14 kDa, as expected, for both Qβ VLPs and Qβ VLPs released

from motors (Figure 2c). Morphologically, Qβ VLPs released from the chitosan motor layer (Figure 2e) showed a monodispersed spherical shape by transmission electron microscopy (TEM) observation, consistent with those found in TEM micrograph of purified Qβ VLPs (Figure 2d). Thus, coating Qβ VLPs on micromotors did not damage the particle integrity. To quantify the amount of released Qβ VLPs from motor, SDS-PAGE densitometry was conducted. To densitometric quantify of Qβ VLP payload from motors, supernatant of dissolved Qβ-motors (PBS, pH=5) at different time points were collected and stained with Coomassie Brilliant Blue following SDS-PAGE. Purified Qβ VLP standards, ranging from 0.26 to 2.6 mg/ml, were denatured and separated in the same gel (Figure 2f). It is worth it to note that analogous studies, carried out with the Qβ VLP-loaded passive microparticles, resulted in a similar release of Qβ payload after 8 h incubation in PBS pH 5.0 (data not shown), as was essential to continue with subsequent *in vitro* and *in vivo* studies. Densitometric volume of Qβ coat protein band was calculated for each sample using ImageJ. As shown in Figure 2g, the results indicated 50% of payload was quickly released within the first half hour, likely due to the powerful propulsion of the motors, and the remaining payload of Qβ VLPs released completely from motors into the solution within 8 hours incubation. Moreover, the Qβ VLP payload release curves were in agreement comparing the data obtained by the two assays and either assay could be used to quantify the payload from different batches samples for further *in vitro* and *in vivo* applications.

Prior to test the Qβ-motor *in vivo*, different *in vitro* studies were performed. Initially, a cytotoxicity assay was performed to test whether Qβ-motor could enhance the phagocytic activity of macrophage against cancer cells. The experimental schematic is shown in Figure 3a. Luciferase-labeled ovarian tumor cells (ID8-Defb29/Vegf-A-luc) were co-cultured with RAW264.7 macrophages at 1: 1 ratio and stimulated with different treatments (as described below). The number of viable tumor cells was determined after 20 h of co-culture by measuring the bioluminescence signals of the tumor cells. Negligible cancer cell phagocytosis was observed in co-culture of macrophages and tumor cells, highlighting the fact that macrophages require stimulation to effective kill tumor cells. We found Qβ VLPs alone promoted macrophages activation to kill tumor cells (13.6% compared to no stimulation). Qβ-motor could significantly promote cytotoxic potential of macrophages by doubling tumor cell killing with an efficacy of 32.2% (Figure 3b and 3c). Qβ VLPs have a highly organized and repetitive structures that could be recognized as potent geometric pathogen-associated molecular pattern (PAMPs) and induce innate immune responses, such as dendritic cells maturation and macrophages phagocytosis.[27] However, as a therapy, VLPs may only be taken up or react with the local cells at the injection site. The fast clearance from the blood by the reticuloendothelial system compromises the therapeutic potentials of VLPs.[28] Qβ-motors broaden the movement area of payload therefore improving the macrophage activation. Bare Mg-based micromotors (motor), passive Mg microparticles fully coated with two layers of TiO_2 (passive control; not displaying self-propulsion due to full coverage of the Mg microparticle), and Qβ VLP-loaded passive microparticles (Qβ-passive control) were used as negative controls. As shown in Figure 3b, neither the motor nor the passive control showed any effect on the tumor cell viability, indicating the cytotoxicity improvement from Qβ-motor is due to the Qβ VLP payload and active delivery, and not due to the other components of the micromotor carrier. Interestingly,

no cytotoxicity improvement was observed from Qβ-passive control. The lack of activity of the Qβ-passive control maybe be explained by aggregation of the large microparticles due to corona formulation; based on the lack of movement there is higher likelihood for aggregation and sedimentation, which may hamper effective Qβ-release and Qβ-cell interactions. No toxicity was observed in tumor cells only after incubation of any stimulation, which again indicated the good biocompatibility of all micromotor compositions (Figure 3b, slash histogram). Cytokine secretion is a typical indication of immune responses.[29,30] Therefore, we next collected the supernatant medium in co-cultured wells after different stimulation and tested the released cytokines in the supernatant using enzyme-linked immunosorbent assay (ELISA). Consistent with the macrophages cytotoxicity results, Qβ-motor activated macrophages released the highest level of proinflammatory immune cytokines, such as Interleukin 6 (IL-6, $p<0.0005$ *vs.* control) and TNF-α ($p<0.0005$ *vs.* control), while Qβ VLP alone only slightly elevated the level of IL-6 ($p<0.05$ *vs.* control) but not TNF-α (Figure 3d). The results demonstrated that the propulsion generated from motors could enhance Qβ VLP distribution in the whole area of the cell culture wells and promote the interaction between Qβ VLP and macrophages for better macrophage activation. Of note, the level of IL-10 was reduced by any stimulation, including negative controls. IL-10 is an immunosuppressive cytokine which could polarize tumor associated macrophages toward a pro-tumor phenotype.[31] As shown in Figure 3d, the level of IL-10 in the non-stimulation control was the highest among all groups. In contrast, motor ($p<0.05$ *vs.* control) and passive control ($p<0.0005$ *vs.* control) downregulated the IL-10 level; and Qβ-passive control, Qβ VLPs, and Qβ-motor further reduced the IL-10 secretion in the co-cultured microenvironment ($p<0.0001$ *vs.* control). Overall, the *in vitro* tests demonstrate that Mg-based micromotors could provide enhanced macrophage activation effect of Qβ VLPs, indicating the potential of immunostimulatory nanostructures loaded motors as tools in tumor immunotherapy.

Before therapeutic experiment, *in vivo* retention of the Qβ-motors in the peritoneal space including tumor ascites was evaluated using an orthotopic murine ovarian tumor model. Here we use a more aggressive ovarian tumor cell line, ID8-Defb29/Vegf-A, to obtain a more angiogenetic and ascetics-rich tumor compared to ID8 parental cell line.[32] C57BL/6J mice were intraperitoneally (i.p.) challenged with luciferase-labeled ID8-Defb29/Vegf-A ovarian tumor cells. On day 35 post tumor inoculation, when tumor-bearing mice had started to develop ascites, mice were i.p. injected with Cy5-labeled Qβ VLPs (Cy5-Qβ VLPs), Cy5-Qβ-passive control, or Cy5-Qβ-motor at the equivalent Qβ dose (320 μg Qβ VLPs). At different time points over a range of 3 days post injection, mice were imaged with an *in vivo* imaging system (IVIS). Figure 4a displayed the fluorescence quantification (quantified as the average radiance (photons/sec/cm^2/sr) of a defined region of interest) of the Cy5-labeled Qβ VLPs retained in the peritoneal space from different treatment groups. Figure 4b showed the representative Cy5 fluorescence images of the treated mice at 8 and 14 h post administration. Free Cy5-Qβ was retained in the peritoneal cavity only the first 8 hours post injection and then rapidly excreted. The Qβ-motor showed both a stronger fluorescent signal overall and a longer retention time of Qβ VLPs in peritoneal space after i.p. injection, indicating the active propulsion of micromotors effectively promote better distribution and longer retention of the payload therapies. A quantitative *ex vivo* organs accumulation of Qβ

VLPs released from motors was then studied to confirm the retention properties of payload released from micromotors within the peritoneal tumors/organs at 24 h post injection. The fluorescence quantification of Cy5-Qβ VLPs retained in tumors tissues and different organs was shown in Figure 4c and the representative bioluminescence intensity (BLI) and fluorescence images of the corresponding organs were shown in Figure 4d. BLI images were used to confirm the tumor tissues (primary and metastases tumors). As observed, besides isolated tumor tissues collected in peritoneal cavity, adherent metastases were found in different organs, such as colons and spleens. While Qβ VLPs alone and Qβ-passive control were excreted rapidly from the mouse body 24 h post administration, Qβ VLPs released from motor was retained in the tumors and major organs in peritoneal cavity (Figure 4c and 4d; it should be noted that at 6 h post administration free Qβ and passive Qβ-control motor also were detected in the liver; thus there is no difference in metabolic clearance, just the rate of clearance). To be specific, Qβ-motor showed higher fluorescence signal from tumors than Qβ VLPs alone and Qβ-passive control. In addition to tumor tissues, Qβ VLPs released from motors showed longer retention time and better distribution in the liver, kidney and colon. The propulsion of Qβ VLP-loaded micromotors in ovarian tumor microenvironment enables effective Qβ VLP diffusion and prolongs the retention time of Qβ VLPs. The effective long-term local retention of Qβ VLPs within the local peritoneal space would be favorable for more efficient immune-stimulation of Qβ VLPS to multiple immune cells activation while avoiding frequent injection and heavy accumulation in normal organs.

Encouraged by the *in vitro* and bio-distribution results, Qβ-motors were then further employed for *in vivo* anti-tumor evaluation. The treatment strategy is shown in Figure 5a, wherein the weekly treatments (i.p.) started on day 7 after tumor cells inoculation (i.p.). A total of 6 time-treatments was conducted. We tracked the tumor burden and therapeutic ability of Qβ-motor by measuring BLI from tumor cells in peritoneal cavity (Figure S3), as well as body weight (Figure 5d) after various treatments. In the PBS treated group, all of mice showed heavy tumor burden on day 37 post inoculation and corresponding BLI (Figure 5b and 5c). The results obtained from mice treated with motor and passive control showed similar BLI of tumor cells compared with PBS control, indicating that the payload carrier whether passive or active has no therapeutic effect. Comparatively, significantly reduction of the signal intensity was found in mice after free Qβ VLPs or Qβ-motor treatments, indicating that prolonged tumor reduction. BLI of mice receiving Qβ-passive control at the same Qβ VLP dose was not significantly reduced. The survival curves (Figure 5e) also showed that the Qβ-passive control appeared to be less effective in tumor treatment compared to soluble Qβ VLP or the Qβ-motor treatments; the reduced efficacy is consistent with the imaging studies which indicate slow or ineffective release of the VLP immunotherapy when passive microparticle carriers are used. The inefficient therapeutic outcome is attributed to the differences in clearance and retention (see Figure 4). Mice receiving the Qβ-motor treatment had reduced tumor burden and prolonged therapeutic outcomes (survival) compared to Qβ VLPs alone, although without statistically significant difference. Therefore, as demonstrated in this i.p. inoculated ovarian tumor model, the Qβ-motor treatment, relieving payload in an active fashion and enabling long-term Qβ VLP retention, appears to be a rather effective therapeutic approach to eliminate primary tumor and metastasis in peritoneal cavity. The consistency of body weight in all other control

groups suggested no appreciable systemic *in vivo* toxicity induced by micromotor or passive control at our experimental dose.

Qβ VLP-based vaccines have shown ability to induce strong humoral and cellular immune responses and their therapeutic potential has been tested in clinical trials in treating melanoma.[33] The promising results from those studies emphasize the powerful immunogenicity of Qβ VLP as an efficient therapeutic vaccine platform to enhance both innate and adaptive arms immune response. Similarly, our group recently found another virus-based nanoparticles, CPMV, have intrinsic immunogenicity and CPMV *in situ* therapy was able to strong antitumor effect in treating ID8-Defb29/Vegf-A murine ovarian tumor model. The mechanism study showed that the virus particles initiated myeloid cells activation and repolarized tumor associated macrophages and neutrophils to an anti-tumor phenotype, and then promoted effector and memory CD4+ and CD8+ T cell responses.[6] To further improve the therapeutic impact of virus particles or VLPs against metastatic ovarian tumor, here we engineered Qβ VLP-loaded micromotors and tested the potential of Qβ-motor in treating ovarian cancer *in vivo*. The enhanced diffusion provided by the active motors comes with the reaction between Mg particles and the acidic IP fluids in tumor microenvironment,[34] providing the micromotors with a propulsion force. The local stimuli triggered propulsion from Mg-based micromotors could allow Qβ-motor to explore larger areas than passive diffusion, improve the chances of interaction between the VLPs and multiple immune cells, and eventually promote extra survival benefit.

3. Conclusion

In this study we have presented an effective method to actively deliver immunotherapeutic VLPs for the treatment of peritoneal ovarian tumors using biocompatible and biodegradable Mg-based micromotors. We have demonstrated that Qβ VLP-loaded Mg micromotors with autonomous propulsion in peritoneal fluid can enhance the immunostimulatory properties of Qβ VLP payload and improve cancer immunotherapy. *In vitro* cellular studies indicated that Qβ-motors can extend the distribution and interaction between Qβ VLPs and macrophages, resulting in a more efficient activation of macrophages. By employing a peritoneal ovarian tumor model, we demonstrated that Qβ-motors actively deliver intact immunostimulatory Qβ VLPs, greatly enhancing the distribution and retention time of the Qβ VLP payload in the tumor microenvironment, leading to suppress the tumor growth in the peritoneal cavity. The presented micromotor-based *in vivo* immunotherapy strategy shows unique advantages over Qβ VLP-loaded passive microparticles, balancing the fast excretion of soluble Qβ VLPs and slow payload release presented by passive vehicles, and thus leading to increased survival rates of tumor-bearing mice. Despite the encouraging results, this micromotor-based VLP-delivery technology is still at an early stage and needs to address important challenges such as scalability issues. Current micromotor manufacture will require high-throughput processes and facilities for their production at a large scale. Future work will also involve full immunological studies and VLP-motor dosage optimizations. Such motor-based VLPs delivery system could also be used as an active immunotherapy tool to target other types of primary and metastatic tumors in the peritoneal cavity.

4. Experimental Section

Qβ expression and purification:

Qβ VLPs were prepared based on a previously published protocol.[35] *E.coli* BL21(DE3) cells were transformed with Qβ plasmid (pET28CP) and plated onto lysogeny broth (LB) agar media (Kanamycin). The next day, isolated colonies were picked from plates into 100 ml selective LB media and grown to saturation for 12 h at 37 °C. A total of 10 mL of culture was then diluted into 1000 mL of freshly prepared selective LB. Culture growth was monitored by optical density at 600 nm (OD600). When the OD600 of the cultures reached approximately 0.8 (mid log phase), protein expression was induced with the addition of 10 mL of 100 mM IPTG, giving a final IPTG concentration of 1 mM. Shaking was continued at 37 °C for an additional 6 h, at which point cells were collected by centrifugation in an Eppendorf A-4–81 rotor at 4000 rpm (4 °C) for 30 min. The supernatant was decanted, and the cell pellet was frozen at −80 °C for 12 h. Cells were then resuspended in ~100 mL of 1× Tris Buffered Saline (TBS), pH 7.4. The buffer used for the original resuspension continued to be used for subsequent steps of particle preparation. Samples were chilled on ice and then sonicated with a probe sonicator (10 min total sonication time, 5 s on and 5 s off, 60–70 W power output) in an ice bath to lyse cells. The cell debris was pelleted in an Eppendorf FA-45–6–30 rotor at 10000 rpm for 10 min, and the supernatant was decanted and collected. The Qβ particles were precipitated from the resulting supernatant by the addition of 10% w/v PEG8000 at 4 °C for 12 h on a rotisserie. The precipitated fraction was isolated from the supernatant by centrifugation in an Eppendorf FA-45–6–30 rotor for 10 min (4 °C) at 10000 rpm. The pellet was redissolved in ~20 mL of TBS and extracted with a 1:1 v/v solution of n-BuOH/$CHCl_3$ to remove excess lipid. The aqueous fraction was collected following centrifugation using a FA-45–6–30 rotor for 10 min, 4 °C at 10000 rpm. Qβ particles were purified on 10–40% sucrose velocity gradients in an SW28 rotor at 28000 rpm for 4.5 h.

Synthesis of Cy3 labeled Qβ particles:

Qβ were covalently labeled with Cyanine3 (Cy3) dye using N-hydroxysuccinimide-activated esters targeting surface-exposed lysine residues on the viral coat proteins (Cy3-NHS ester was obtained from Lumiprobe). 1mg Qβ were incubated with 0.1 mg Cy3-NHS ester in 0.1 M phosphate buffer (pH=8.4) at room temperature for 4 hours. Cy3-Qβ were then purified by overnight dialysis.

Characterization of Qβ particles:

Size exclusion chromatography (SEC) analysis of Cy3-Qβ. 100 μL of Cy3-Qβ (1 mg/mL) were injected into a Superose 6 column on an AKTA Explorer chromatography system (GE Healthcare) at a flow rate 0.5 mL/min in 10 mM KP buffer (pH 7.4) and recorded the absorbance at 260, 280 and 554 nm.

Non-denaturing Agarose gel electrophoresis.—20 μg of each sample (in 6x loading dye) were fractionated by 0.8% (w/v) agarose gel electrophoresis at 100 V for 60 min in Tris borate EDTA (TBE) buffer. Gels were visualized under UV light and after staining with 0.25% (w/v) Coomassie Brilliant Blue.

Denaturing gel electrophoresis (SDS-PAGE).—20 μg of each sample were denatured 100°C for 5 min in 4× LDS loading dye (Thermo Fisher Scientific). The denatured samples were fractionated in 12% NuPAGE precast gels in 1×MOPS buffer (Thermo Fisher Scientific) at 200 V for 40 min. Gels were photographed before and after staining with 0.25% w/v Coomassie Brilliant Blue using the FluorChem R imaging system (Protein Simple, San Jose, CA) under white light.

Transmission electron microscope (TEM) analysis.—TEM was performed using a FEI Tecnai Spirit G2 BioTWIN (FEI, Hillsboro, OR). Samples (0.5–1 mg/ml) were mounted on 400-mesh hexagonal copper grids bearing Formvar support film, stained with 2% uranyl acetate, and allowed to dry for 12 h.

Quantification of Qβ released from Qβ-motor.

To quantify the amount of released Qβ, 2 mg of Qβ-motors were dissolved in 300 μL of PBS (pH=5) and the released Qβ in the supernatant was collected by centrifugation at different time intervals (0.5, 1, 2, 4, and 8 h). 20 μL of each timepoint sample or standard Qβ solution (0.26, 0.52, 1.3 and 2.6 mg/mL) were denatured and fractionated in single piece 12% NuPAGE precast gel in 1×MOPS buffer at 200 V for 40 min. Gels were photographed before and after staining with 0.25% w/v Coomassie Brilliant Blue using the FluorChem R imaging system (Protein Simple, San Jose, CA) under white light. Standard curve was established based on the densitometric volume of standard Qβ solution using ImageJ. Then the concentration of Qβ coat protein band was calculated for each sample accordingly.

Synthesis of Qβ-motors:

The Mg-based micromotors were prepared using magnesium (Mg) microparticles (catalog #FMW20, TangShan WeiHao Magnesium Powder Co.; average size, 20±5 μm) as the core. These Mg microparticles were initially washed with acetone to eliminate the presence of impurities. After being dried under a N_2 current, the Mg microparticles were dispersed onto glass slides, followed by a gold sputtering (over the exposed Mg microparticle) performed in a Denton Discovery 18 instrument at room temperature for 3 s under vacuum of 5×10−6 Torr, DC power 200 W, Ar flow of 2.8 mT, and rotation speed of 13 rpm. The micromotors were then exposed to an atomic layer deposition (ALD) of TiO_2 (at 100 °C for 1000 cycles) using a Beneq TFS 200 system. Since ALD is a chemical vapor deposition technique, utilizes gas phase reactants, it leads to uniform coatings over the Mg microparticles, while still leaving a small opening (~2 μm) at the contact point of the microparticle to the glass slide, as desired for the reaction with the IP fluid. After that, the micromotors were coated with 2 protective layers of 120 μL of 1% (w/v) PLGA (Sigma-Aldrich, P2191) prepared in ethyl acetate (Sigma-Aldrich, 270989). The micromotors were then loaded with Qβ (100–320 μg, depending of the study) using a 0.05% (w/v) chitosan (Sigma-Aldrich, C3646) coating prepared in water and containing 0.1% (w/v) sodium dodecyl sulfate (SDS) (Sigma-Aldrich, 62862) and 0.02% (v/v) acetic acid (Sigma-Aldrich, 695092), forming the outermost layer coated on the Mg-based micromotors. Finally, the Qβ-motors were collected by lightly scratching the motors off the glass slide and they were stored at 4 °C.

Synthesis of passive controls:

The negative passive controls consisted on passive Mg microparticles fully coated *via* ALD (at 100 °C for 1000 cycles) with two layers of TiO_2 and loaded (Qβ-passive control) or not (passive control) with Qβ following the same protocol described above. The two layers of TiO_2 fully coat the Mg, avoiding its reaction with IP fluid.

Synthesis of Cy3-labeled Qβ-motors:

For characterizing the Qβ-motors, fluorescent micromotors were prepared following the same protocol described above but loading the chitosan layer with a Cy3-labeled Qβ (Cy3 dye, λ_{ex}=554 nm/ λ_{em}=568 nm).

Synthesis of Cy5-labeled Qβ-motors:

For the *in vivo* retention study, fluorescent micromotors were prepared following the same protocol described above but loading the chitosan layer with a Cy5-labeled Qβ (Cy5 dye, λ_{ex}=649 nm/ λ_{em}=666 nm). To compare with the Cy5- Qβ-motors, Cy5-Qβ-passive Mg microparticles fully coated with two layers of TiO_2 were used, following the same loading protocol.

Micromotor propulsion studies:

Autonomous Mg-based micromotors propulsion was obtained by placing the different motor formulations in mouse IP fluid (obtained from tumor-bearing mice on day 30 after tumor inoculation). An inverted optical microscope (Nikon Eclipse 80i upright microscope) coupled with different microscope objectives (20× and 40×) and a QuantEM 512/SC camera were used for recording the autonomous micromotor propulsion in the IP fluid. The speed of the ~25 μm Mg-based micromotors was characterized using the MetaMorph 7.1 software (Molecular Devices, Sunnyvale, CA) being expressed in μm/s.

Micromotor characterization:

Bright field, fluorescent and merged images of the Cy3-Qβ and Cy5-Qβ-loaded Mg-based micromotors and passive Mg microparticles were captured using an EVOS FL microscope coupled with a 20× and 40× microscope objectives and fluorescence filters for red light excitation.

Scanning electron microscopy (SEM) images of the Mg-based micromotors were obtained with a FEI Quanta 250 ESEM instrument (Hillsboro, Oregon, USA), using an acceleration voltage of 10 kV. EDS mapping analysis was performed using an Oxford EDS detector attached to SEM instrument and operated by Pathfinder software.

Mice and Cell lines:

Female C57BL/6 mice (6- to 8-week old) were purchased from The Jackson Laboratory. All mouse studies were performed in accordance with UCSD's Institutional Animal Care and Use Committee. Macrophage cells (RAW 264.7, ATCC) were maintained in Dulbecco's minimal essential medium (DMEM) supplemented with 10% (v/v) heat-inactivated fetal bovine serum (FBS) and 1% (v/v) penicillin-streptomycin. ID8-Defb29/Vegf-A cells (a gift

from Dr. Steve Fiering, Dartmouth College) were maintained in RPMI 1640 medium supplemented with 10% (v/v) heat-inactivated FBS, 1 mM sodium pyruvate, 0.05 mM 2-mercaptoethanol, and 1% (v/v) penicillin-streptomycin. Cells were maintained at 37 °C in a 5% CO_2 humidified air environment.

In vitro cytotoxicity assay and cytokine measurement:

ID8-Defb29/Vegf-A cells were transfected with luciferase (ID8-Defb29/Vegf-A-luc) as previously described.[36] RAW 264.7 macrophages and ID8-Defb29/Vegf-A-luc cells were plated in 96-well plates with 1:1 ratio. Cells were treated with 0.13 mg of motors (10 μL PBS pH=5), Passive control (10 μL PBS pH=5), Qβ-motor (10 μg Qβ, 10 μL PBS pH=5), Qβ-passive control (10 μg Qβ, 10 μL PBS pH=5), or 10 μg Qβ (10 μL PBS pH=5) for 20 h. Supernatants of co-culture samples were collected and tested by enzyme-linked immunosorbent assay (ELISA) to detect IL-6, tumor necrosis factor α (TNF-α), and IL-10 (BioLegend, San Diego, CA) according to the manufacturer's instruction. Non-adherent cells were washed with medium. After adding luciferin (0.15 mg/ml), the cells were imaged in a Xenogen IVIS 200 Optical Imaging System (Caliper Life Sciences, Hopkinton, MA). Total bioluminescence was determined by a Living Image software (PerkinElmer, Waltham, MA). Regions of interest were quantified as average radiance (photons/sec/cm^2/sr).

In vivo micromotor biodistribution:

All experiments were conducted in accordance with UCSD's Institutional Animal Care and Use Committee. Mice were intraperitoneally (i.p.) implanted with 2×10^6 ID8-Defb29/Vegf-A-luc cells. After 30–35 days, mice were divided into required groups according to bioluminescence signals from tumor cells using IVIS imaging. Grouped mice were i.p. injected with Cy5-Qβ (320 μg), Cy5-Qβ-passive control (320 μg Qβ), or Cy5-Qβ-motor (320 μg Qβ). Fluorescence imaging (Far-red filter set, 10 s exposure) and bioluminescence imaging (3 min exposure) were conducted at different time points. Tumor and major organs in peritoneal cavity (spleen, kidney, liver, and colon) were excised after 24 h and analyzed by *ex vivo* imaging. Regions of interest were quantified as average radiance (photons/sec/cm^2/sr).

In vivo micromotor ovarian tumor treatment:

2×10^6 live cells/200 μL PBS were implanted into mice by i.p. injection. On day 7 of tumor growth, tumor bearing mice were weekly i.p. injected with 320 μg of Qβ in 200 μl PBS, 2.5 mg motor, 2.5 mg passive control, 2.5 mg Qβ-passive control (320 μg Qβ), 2.5 mg Qβ-motor (320 μg Qβ), or PBS only for a total of 6 doses. Tumor growth was also monitored by total bioluminescence imaging and body weight. Mice were i.p. injected with luciferin (150 mg/kg, Thermo Fisher Scientific, Waltham, MA) and imaged in a Xenogen IVIS 200 Optical Imaging System (Caliper Life Sciences, Hopkinton, MA). Mice were euthanized when weight reached to 35 grams or when moribund.

Supplementary Material

Refer to Web version on PubMed Central for supplementary material.

Acknowledgements

This work was supported in part by a grant from the National Institute of Health, NCI Alliance for Cancer Nanotechnology (U01CA218292 to N.F.S.) and a grant from the Defense Threat Reduction Agency Joint Science and Technology Office for Chemical and Biological Defense (Grant Number HDTRA1-14-1-0064). M. A. L-R. acknowledges the UC MEXUS-CONACYT Doctoral Fellow. R. M-U. acknowledges the support from the Fulbright grants and the Conicyt PFCHA/Doctorado becas Chile/2015-56150011.

References

[1]. Schumacher TN, Schreiber RD, Science 2015, 348, 69. [PubMed: 25838375]

[2]. Ribas A, Wolchok JD, Science 2018, 359, 1350. [PubMed: 29567705]

[3]. Halperin SA, Ward B, Cooper C, Predy G, Diaz-Mitoma F, Dionne M, Embree J, McGeer A, Zickler P, Moltz KH, Martz R, Meyer I, McNeil S, Langley JM, Martins E, Heyward WL, Martin JT, Vaccine 2012, 30, 2556. [PubMed: 22326642]

[4]. Huber B, Schellenbacher C, Jindra C, Fink D, Shafti-Keramat S, Kirnbauer E, PLoS ONE 2015, 10, e0120152.

[5]. Lizotte PH, Wen AM, Sheen MR, Fields J, Rojanasopondist P, Steinmetz NF, Fiering S, Nat. Nanotechnol 2016, 11, 295. [PubMed: 26689376]

[6]. Wang C, Fiering S, Steinmetz NF, Adv. Therap 2019, 1900003.

[7]. Kerstetter-Fogle A, Shukla S, Wang C, Beiss V, Harris PLR,; Sloan AE, Steinmetz NF, Cancers 2019, 11, 515.

[8]. Hoopes PJ, Wagner RJ, Duval K, Kang K, Gladstone DJ, Moodie KL, Crary-Burney M, Ariaspulido H, Veliz FA, Steinmetz NF, Fiering S, Mol. Pharm 2018, 15, 3717. [PubMed: 29613803]

[9]. Maphis NM, Peabody J, Crossey E, Jiang S, Jamaleddin Ahmad FA, Alvarez M, Mansoor SK,Yaney A, Yang Y, Sillerud LO, Wilson CM, Selwyn R, Brigman JL, Cannon JL, Peabody DS, Chackerian B, Bhaskar K, NPJ Vaccines 2019, 4, 26. [PubMed: 31231552]

[10]. O'Rourke JP, Peabody DS, Chackerian B, Curr. Opin. Virol 2015, 11, 76. [PubMed: 25829254]

[11]. Mohsen MO, Speiser DE, Knuth A, Bachmann MF, WIREs Nanomed. Nanobiotechnol 2019, e1579.

[12]. Liao JB, Disis ML, Gynecol. Oncol 2013, 130, 667. [PubMed: 23800697]

[13]. Wilhelm S, Tavares AJ, Dai Q, Ohta S, Audet J, Dvorak HF, Chan WW, Nat. Rev. Mater 2016, 1,16014.

[14]. Wang J, Nanomachines: Fundamentals and Applications. Wiley-VCH: Weinheim 2013.

[15]. Li JX, Esteban-Fernandez de Avila B, Gao W, Zhang LF, Wang J, Sci. Robot 2017, 2, eaam6431.

[16]. Abdelmohsen LKEA, Peng F, Tu Y, Wilson DA, J. Mater. Chem. B 2014, 2, 2395. [PubMed: 32261411]

[17]. Wang H, Pumera M, Adv. Funct. Mater 2018, 28, 1705421.

[18]. Felfoul O, Mohammadi M, Teherkhani S, de Lanauze D, Xu YZ, Loghin D, Essa S, Jancik S, Houle D, Lafleur M, Gaboury L, Tabrizian M, Kaou N, Atkin M, Vuong T, Batist G, Beauchemin N, Radzioch D, Martel S, Nat. Nanotechnol 2016, 11, 941. [PubMed: 27525475]

[19]. Hortelão AC, Patiño T, Perez-Jiménez A, Blanco À, Sánchez S, Adv. Funct. Mater 2018, 28, 1705086.

[20]. Esteban-Fernandez de Avila B, Angsantikul P, Li JX, Gao W, Zhang LF, Wang J, Adv. Funct. Mater 2018, 28, 1705640.

[21]. Chen CR, Karshalev E, Guan JG, Wang J, Small 2018, 14, 1704252.

[22]. Esteban-Fernandez de Avila B, Angsantikul P, Li JX, Lopez-Ramirez MA, Ramirez-Herrera DE, Thamphiwatana S, Chen CR, Delezuk J, Samakapiruk R, Ramez V, Zhang LF, Wang J, Nat. Commun 2017, 8, 272. [PubMed: 28814725]

[23]. Gao R, Dong R, Thamphiwatana S, Li J, Gao W, Zhang L, Wang J, ACS Nano 2015, 9, 117. [PubMed: 25549040]

[24]. Gao W, Feng X, Pei A, Gu Y, Li J, Wang J, Nanoscale 2013, 5, 4696. [PubMed: 23640547]

[25]. Sogias IA, Khutoryanskiy VV, Williams AC, Macromol. Chem. Phys 2010, 211, 426.

[26]. Golmohammadi R, Fridborg K, Bundule M, Valegård K, Liljas L, Structure 1996, 4, 543. [PubMed: 8736553]

[27]. Bachmann MF, Jennings GT, Nat. Rev. Immunol 2010, 10, 787. [PubMed: 20948547]

[28]. Almeida JP, Chen AL, Foster A, Derzek R, Nanomedicine (Lond) 2011, 6, 815. [PubMed: 21793674]

[29]. Lacy P, Stow JL, Blood 2011, 118, 9. [PubMed: 21562044]

[30]. Van der Meide PH, Schellekens H, Biotherapy 1996, 8, 243. [PubMed: 8813336]

[31]. Chuang Y, Knickel BK, Leonard JN, Innate Immun. 2016, 22, 647. [PubMed: 27670945]

[32]. Conejo-Garcia JR, Benencia F, Courreges MC, Kang E, Mohamed-Hadley A, Buckanovich RJ, Holtz DO, Jenkins A, Na H, Zhang L, Wagner DS, Katsaros D, Caroll R, Coukos G, Nat Med. 2004, 9, 950.

[33]. Goldinger SM, Dummer R, Baumgaertner P, Mihic-Probst D, Schwarz K, Hammann-Haenni A, Willers J, Geldhof C, Prior JO, Kundig TM, Michielin O, Bachmann MF, Speiser DE, Eur. J. Immunol 2012, 42, 3049. [PubMed: 22806397]

[34]. Xu L, Fidler IJ, Can. Res 2000, 60, 4610.

[35]. Isarov SA, Lee PW, Pokorski JK, Biomacromolecules 2016, 17, 641. [PubMed: 26765848]

[36]. Wang C, Veronique B, Steinmetz NF, JVI. 2019, 93, 00129–19.

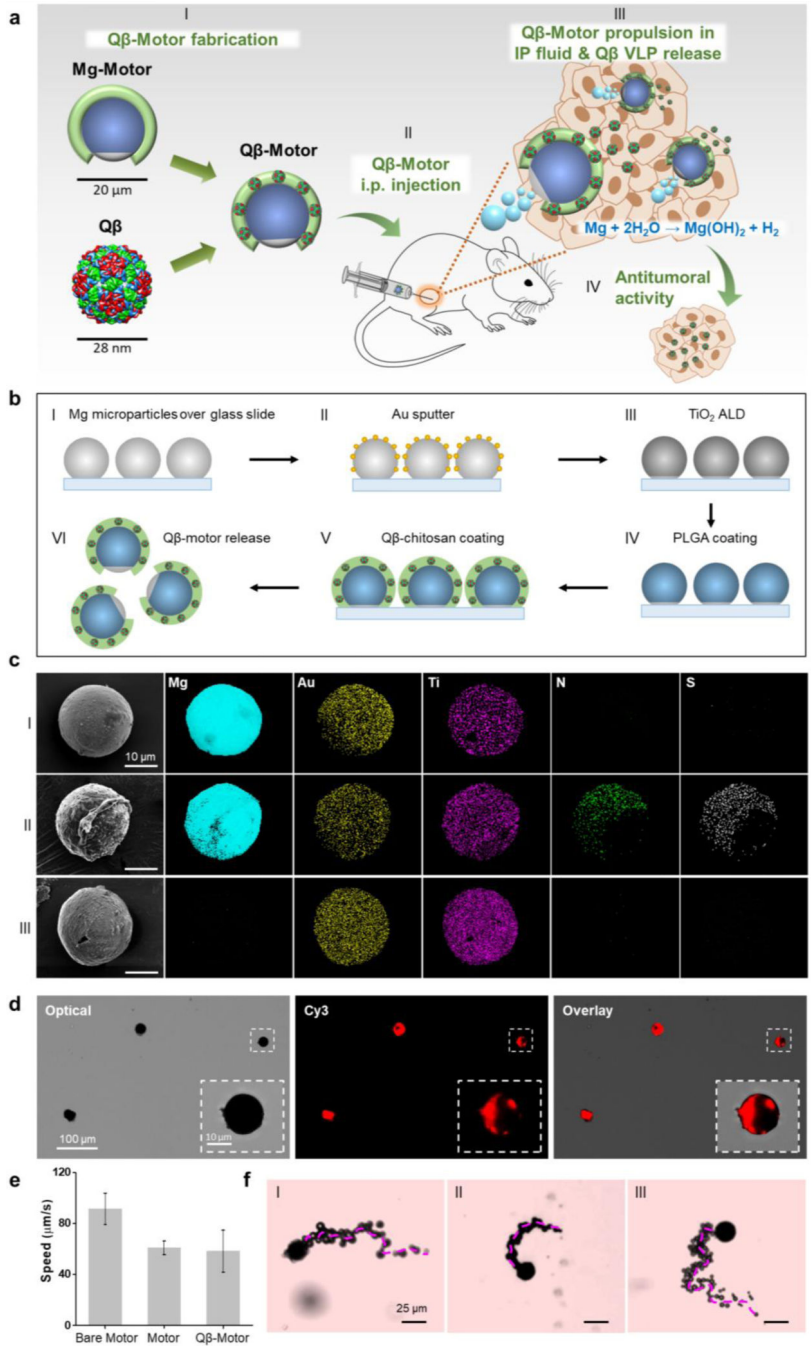

Figure 1. Qβ-motors towards active enhanced therapy of ovarian cancer: concept, preparation, structural and propulsion characterization.

(a) Schematic (not to real scale) of the fabrication, *in vivo* administration and in *vivo* actuation of Qβ-motors as an active Qβ VLP release alternative in ovarian tumor. (b) Schematic (not to real scale) of the Qβ-motors preparation: (I) 25 μm Mg microparticles are spread over glass slides, (II) gold sputter over the Mg microparticles, (III) TiO_2 atomic layer deposition (ALD), (IV) PLGA coating layer over the Mg/Au/TiO_2 micromotors, (V) Qβ VLP-loaded chitosan film over the Mg/Au/TiO_2/PLGA micromotors, and (VI) release of the resulting Qβ-motors. (c) Scanning electron microscopy (SEM) images of a Mg/Au/TiO_2/

PLGA micromotor, Mg/Au/TiO_2/PLGA/ Qβ VLP-loaded Chitosan micromotor, and the Au/TiO_2 shell of a Qβ-motor after being exposed to IP fluid (I-III, respectively) and Energy-dispersive X-ray spectroscopy (EDX) images illustrating the distribution of elemental Mg (cyan), Au (yellow), Ti (magenta), N (green) and S (white). (d) Demonstration of Cy3-labeled Qβ VLP loading in the chitosan film. Microscopy images (optical, fluorescence, and overlay) demonstrating the loading of the Cy3-Qβ VLPs over the Mg-based micromotors. (e) Comparison of the speed of the bare (Mg/Au/TiO_2-motor; without the PLGA and the Chitosan layers), Mg/Au/TiO_2/PLGA/Chitosan-motor and of the Qβ-motor (Mg/Au/TiO_2/PLGA/Qβ@Chitosan-motor) in mouse IP fluid. (f) Microscopic images (corresponding to Video S1) displaying the motion of a (I) Mg/Au/TiO_2-motor, (II) Mg/Au/TiO_2/PLGA/Chitosan-motor and (III) Qβ-motor.

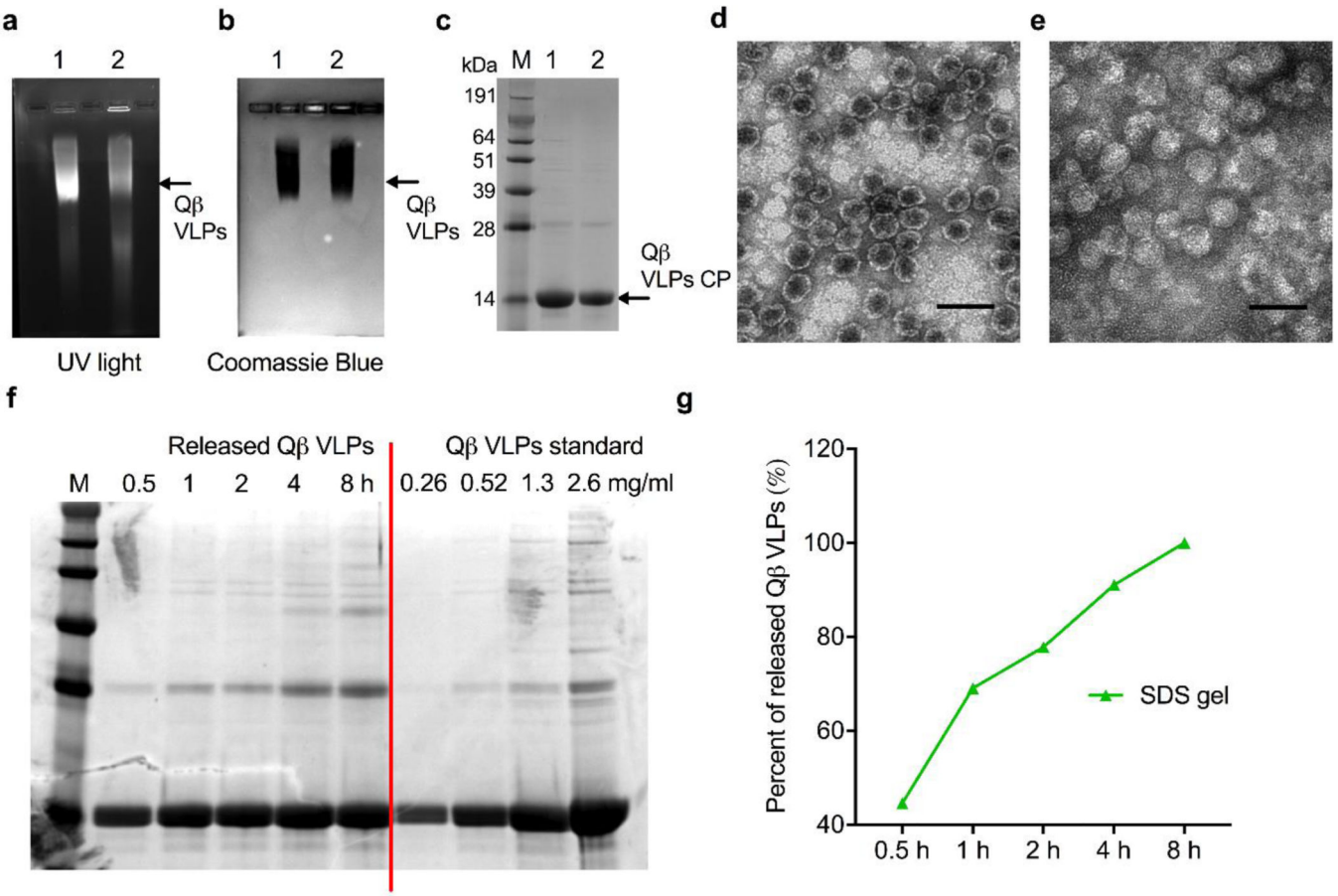

Figure 2. Characterization of Qβ VLPs and Qβ VLPs released from Qβ-motor.

a-b Non-denaturing agarose gel of 20 μg Qβ VLPs or Qβ VLPs released from motor. GelRed nucleic acid gel under UV light (**a**) and staining with Coomassie Brilliant Blue (CBB). The GelRed stains host RNA packaged during VLP assembly and CBB stains the capsid proteins; the gel images are consistent with intact Qβ VLP preparations (**b**). **c** SDS gels of 20 μg Qβ VLPs or Qβ VLPs released from motor following electrophoresis and staining with Coomassie Brilliant Blue. Lanes: M = SeeBlue Plus2 molecular weight marker, 1=Qβ VLPs, 2=Qβ VLPs released from motor; CP = coat protein. **d-e** Transmission electron microscopy (TEM) of Qβ VLPs (**d**) and Qβ VLPs released from Qβ-motor (**e**). Scale bar = 50 nm. **f-g** Quantification of Qβ VLPs released from motor. 2 mg Qβ-motor were dissolved in 300 μl PBS (pH=5) and the released Qβ from the motors was collected at different time intervals (0.5, 1, 2, 4, and 8h). **f** SDS gel of the released samples and standard Qβ VLPs and staining with Coomassie Brilliant Blue. **g** Densitometry (based on band density from **f**) were used to quantify the released Qβ VLPs from motor.

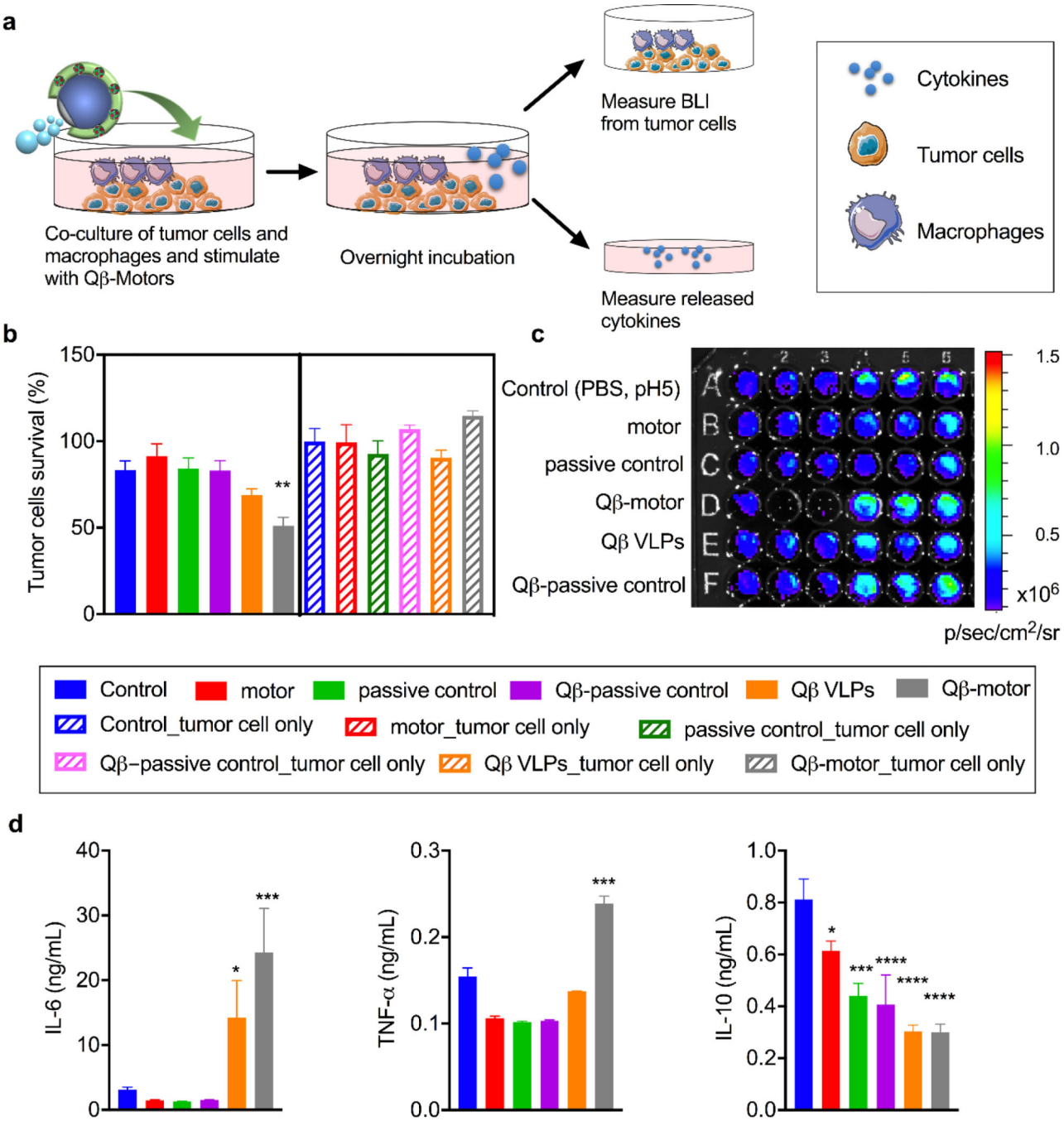

Figure 3. Tumor cytotoxicity improved by Qβ-motor.

a Schematic of *in vitro* tumor cytotoxicity assay. Murine macrophage (RAW 264.7) were co-cultured with ovarian tumor cells (ID8-Defb29/Vegf-A-Luc) with 1:1 ratio. 0.13 mg of motor (10 μL PBS pH=5), passive control (10 μL PBS pH=5), Qβ-motor (10 μg Qβ VLPs, 10 μL PBS pH=5), Qβ-passive control (10 μg Qβ VLPs, 10 μL PBS pH=5), or 10 μg Qβ VLPs (10 μL PBS pH=5) were added as treatment for 20 h. **b** Bioluminescence intensity (BLI) was measured to quantify the percentage of live/dead ID8-Defb29/Vegf-A cells by phagocytosis. Tumor cells only stimulated with different treatments were conducted as

control (slash). **c** Representative IVIS image of co-cultured cells treated with 10 μl PBS (pH=5) as control (A), motor (B), passive control (C), Qβ-motor (D), Qβ VLPs (E), and Qβ-passive control (F). Column 1–3: tumor cells and macrophage co-cultured; column 4–6: tumor cells only. **d** The supernatant of each well was collected and released cytokines (IL-6, TNF-α and IL-10) were measured using ELISA. Data are means ± SEM (n=3). Statistical significance was calculated by one-way ANOVA with Tukey test. *p<0.05, *p<0.01, ***p<0.0005, ****p<0.0001.

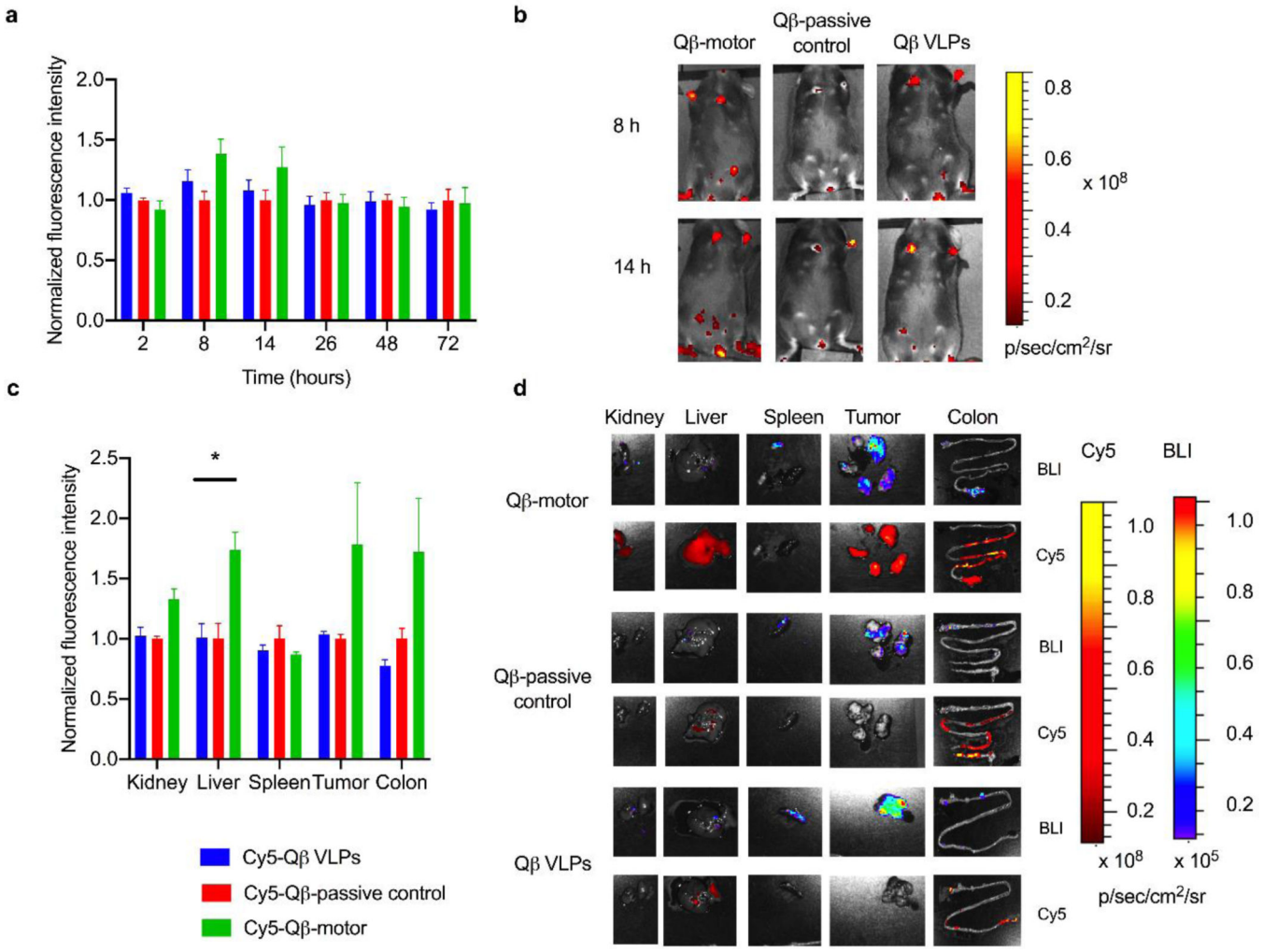

Figure 4. Qβ VLPs released from motor remain inside the peritoneal cavity longer than soluble Qβ VLPs. C57BL/6J mice (n=3) were intraperitoneally injected with Cy5-Qβ VLPs, Cy5-Qβ-passive control, or Cy5-Qβ-motor at t=0 h. Mice were imaged with IVIS imaging system at t=2, 8, 14, 26, 48, and 72 h.

a The normalized fluorescence intensity of Cy5-Qβ VLPs, Cy5-Qβ-passive control, and Cy5-Qβ-motor in the target ROI at different time points and **b** Representative images of each group at t=8 and 14 h. **c** The normalized fluorescence intensity in different organs at 24 h after intraperitoneal injection of with Cy5-Qβ VLPs, Cy5-Qβ-passive control, or Cy5-Qβ-motor. **d** Representative IVIS images of organs at 24 h after treatment. Upper: bioluminescence signal; bottom: Cy5 signal. Data are means ± SEM (n=3). The average radiance was normalized with the Cy5-Qβ-passive control. Statistical significance was calculated by one-way ANOVA followed by Tukey post-hoc test: *p<0.05.

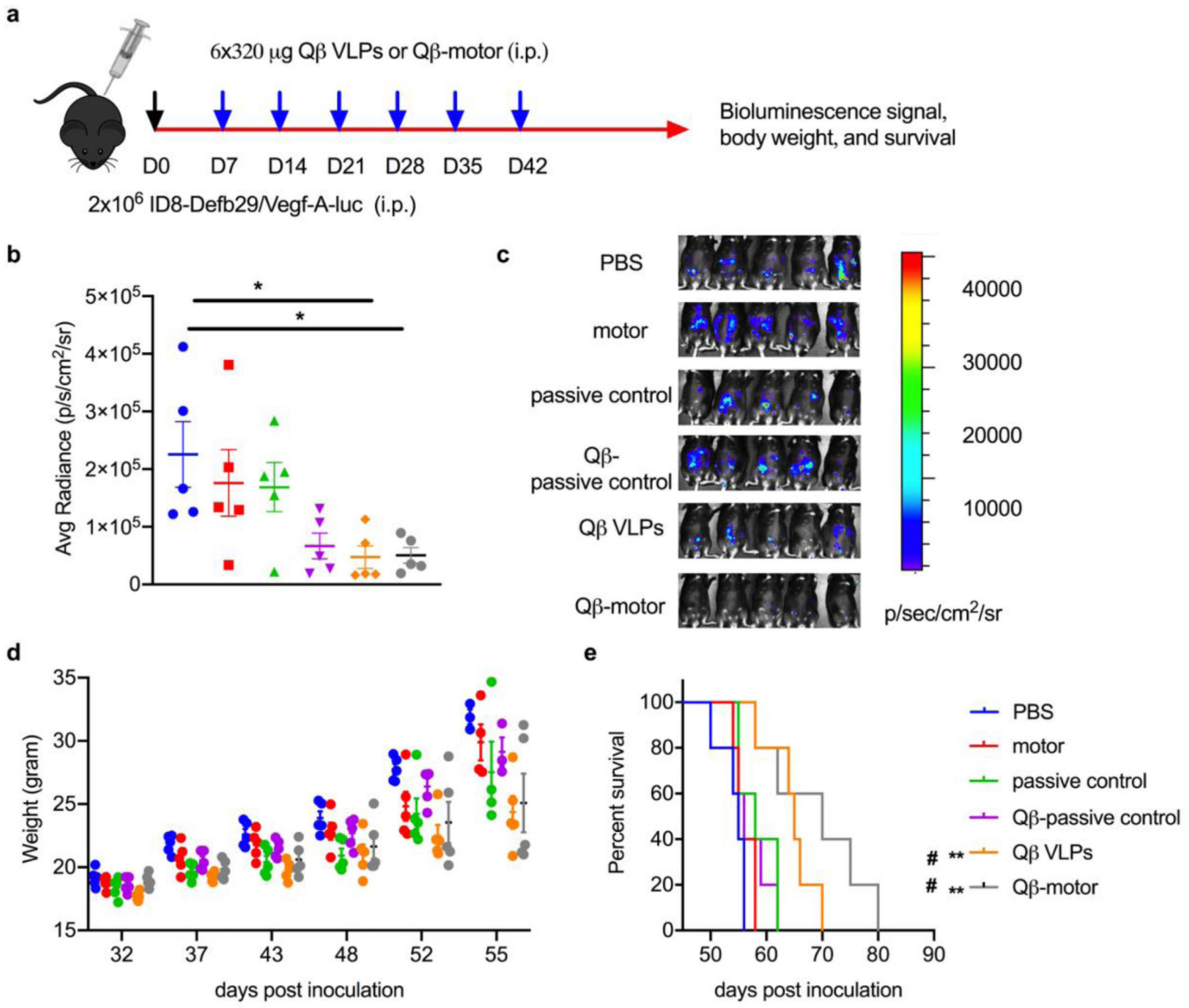

Figure 5. Qβ-motor promotes extra survival benefit in treating aggressive ovarian tumor.

a Schematic of treating schedule in ID8-Defb29/Vegf-A ovarian tumor model. C57BL/6J mice (n=5) were intraperitoneally (i.p.) inoculated with luciferase labeled ID8-Defb29/Vegf-A cells (2×10^6) on day 0. On day 7 of tumor growth, tumor bearing mice were weekly i.p. injected with 320 μg of Qβ VLPs in 200 μL PBS, 2.5 mg motor, 2.5 mg passive control, 2.5 mg Qβ-passive control (320 μg Qβ VLPs), 2.5 mg Qβ-motor (320 μg Qβ VLPs), or PBS only for a total of 6 doses. **b-c** IVIS images of the growth of luciferase-expressing ID8-Defb29/Vegf-A tumors on day 37 post tumor inoculation. (**c**) The average luciferase expression in the peritoneal cavity (**b**). Data are means ± SEM (n=5). Statistical significance was calculated by one-way ANOVA followed by Tukey post-hoc test: *p<0.05. **d** Tumor growth was also followed by measuring the body weight. Mice were sacrificed when weight ≥ 35 grams or when moribund. **e** Survival curves of treated mice. Statistical significance was

calculated using the Mantel-Cox log-rank test: **p<0.01 compared with PBS group; #p<0.05 compared with Qβ-passive control group.